**Menemui Matematik**
**(Discovering Mathematics)**

journal homepage: https://persama.org.my/dismath/home

# Mixed Convection Stagnation-Point Flow with the Presence of Convective Boundary Condition and Radiation Effect

**Muhammad Nazrul Fahmi Zulkefli[1] and Fadzilah Md Ali[2*]**

[1,2]*Department of Mathematics, Faculty of Science, Universiti Putra Malaysia, 43400 UPM Serdang, Selangor*

fadzilahma@upm.edu.my
*Corresponding author

*Received:20 May 2025*
*Accepted: 13 August 2025*

## ABSTRACT

The problem of mixed convection stagnation-point flow on a vertical stretching sheet with three main effects; the external magnetic field, convective boundary condition and radiation is studied. The partial differential equations are reduced to ordinary differential equations using similarity transformation. The transformed boundary layer equations are solved numerically via bvp4c in MATLAB software. The effect of different values of Hartmann number, Biot number and radiation parameter on the skin friction coefficient and local Nusselt number, velocity and temperature profiles are presented and discussed. These effects are also considered for both assisting and opposing flows. Numerical comparison with previous study achieved excellent agreement for both assisting and opposing flows, respectively. Dual solutions are found to exist in the opposing flow only, while unique solutions are obtained for assisting flow. The Biot number and Hartmann number delay the boundary layer separation, while radiation parameter enhances the boundary layer separation

**Keywords: Biot number, Convective boundary condition, Mixed convection, Stagnation-point**

## INTRODUCTION

Applications in engineering and industrial process related to fluid flow has become an important topic among the practitioners. The fluid flow near a stagnation-point practically applied in some real-world problems such as nuclear reactor cooling system. Other than that, various propulsion devices or aircraft and gas turbines are involved with the fluid flow study. Magnetohydrodynamic (MHD) usually be used to demonstrate an investigation on the conductivity and electrically accompanying fluid in magnetic field (Arulmozhi et al., 2022). It was found that the local skin friction coefficient will increase significantly in fluid with the presence of magnetic field. According to Motozawa et al. (2010), the experiment showed that the positive impact towards the heat transfer coefficient due to the magnetic field, and concluded that the heat transfer coefficient increases with magnetic field.

Further study by Ferdows et al. (2022) reflected an agreement to Motozawa et al. (2010) by reaching a conclusion that the magnetic field can give positive impact to the rate of heat transfer and temperature. Ali et al. (2011) studied the effect of an induced magnetic field on the MHD boundary layer flow and heat transfer towards a stretching sheet. The results showed significant result towards the skin friction coefficients as the induced magnetic field increase.

A high interest arises regarding the association between the heat transfer with thermal radiation effect and fluid flow. Extended research considering radiation effect on the fluid flow provides crucial values in high operating temperature as described by Seddeek (2002). Ishak (2011) examined the radiation effect on MHD flow to an exponentially stretching sheet. It was found that the radiation and magnetic parameter will decrease the heat transfer rate at the surface. Das (2014) investigated the radiation and melting effects on MHD flow over a moving surface. The study concluded that increment of thermal radiation will decelerate the fluid velocity and the boundary layer thickness. Further, the study of mixed convection stagnation-point flow over a vertical stretching sheet with external magnetic field and radiation effect done by Ali et al. (2021), mentioned that dual solutions exist for opposing flow and radiation found to retard the separation of boundary layer.

The effect of convective boundary conditions is quantified by parameter named Biot number, where the Biot number represents the ratio of conduction resistance within the body to convection resistance at the surface of the body. Some studies related to Biot number done by previous researchers, for instance Aziz (2009), Hayat et al. (2017), Yahaya et al. (2024) and so forth. Hayat et al. (2017) used Jeffrey liquid in analysing the mixed convection flow by an impermeable inclined stretching cylinder with radiation effects and the convective boundary conditions at the surface. The temperature and concentration were founded to increase as the Biot number became larger. An analysis of the mixed convection flow of a hybrid nanofluid over a permeable stationary cone conducted by Yahaya et al. (2024) considering the effects of thermal radiation and convective boundary condition has yields new physically significant result and concluded that the local Nusselt number is raised by the increment of the Biot number and thermal radiation parameter.

Convective boundary condition is mostly used to define a linear convective heat exchange condition for one or more algebraic entities in thermal (Akbar et al., 2013). The initial concept of convective boundary condition was discussed by Aziz (2009). Similarity, solution for Blasius flow of viscous fluid with convective boundary conditions was presented. The study found the condition which the convection heat transfer coefficient must meet for a similarity type solution to exist. Further, Makinde and Aziz (2010) investigated MHD mixed convection flow in a vertical plate in a porous medium with convective boundary condition was considered. The results reveal that both the fluid velocity and temperature increase with the convective heat transfer parameter or the Biot number. Later, Makinde and Aziz (2011) investigated the effect of a convective boundary condition on boundary layer flow, heat transfer and nanoparticle fraction over a stretching surface in nanofluid. Makinde and Aziz (2011) revealed that reduced Nusselt number and the surface temperature increase with Biot number from 1 to 10, however, only minor effect was observed for Biot number from 10 to 100.

Numerical investigation by Reddy et al. (2018) analysed the impact of key parameters such as magnetic field, thermal radiation and first order chemical reaction over a vertical cone through nanofluid saturated porous medium under convective boundary condition. The study concluded that increasing the values of Biot number has heightens the temperature and concentration of the fluid in the boundary layer regime. Analysis of the mixed convection hybrid nanofluid flow over a stationary cone with thermal radiation and convective boundary condition (Yahaya et al., 2024) found significant results for both assisting and opposing flows. The velocity profile becomes lower with the increase of the Biot number and thermal radiation parameters for opposing flow, which then provide a favourable impact on the local Nusselt number.

Some applications of Biot number in engineering, namely, to examine the effectiveness of insulation and heat exchangers. This is done to ensure that the systems designed are at optimal

thermal performance. Due to the importance of the Biot number, this present study aims to extend the work proposed by Ali et al. (2021) by considering the convective boundary condition. This problem has not yet been taken into consideration, as far as we aware. Therefore, the results that have been reported are new.

## MATHEMATICAL FORMULATION

In this study, we consider the steady two-dimensional boundary layer flow of viscous fluid over a vertical plate surface. The following are the assumptions that has been considered to construct the governing equations. The velocity of far flow on the stretching surface is assumed to be $u_e(x) = ax$ and the surface is stretched with velocity of $u_w(x) = cx$ with $a$ and $c$ are positive constant. It is also assumed that the magnetic Reynolds number is very small, thus and the induced magnetic field can be neglected. The external magnetic field with constant strength, $H_0$ is applied normal to the stretching surface. The plate temperature, $T_w$ resulted from convective heating with temperature $T_f$ and heat transfer coefficient, $h_f$.

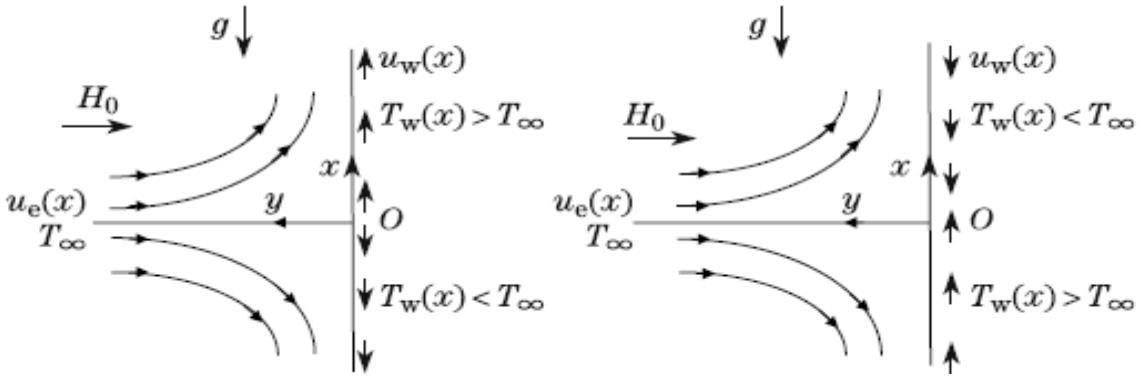


(a) Assisting flow (b) Opposing flow

**Figure 1:** Physical model and coordinate system

Figure 1 explains the vertical stretching sheet in a schematic diagram. Cartesian coordinates ($x$, $y$) are taken with $x$-axis is measured along the sheet oriented in the upward direction, and the $y$-axis is normal to it. The temperature of the plate is assumed as $T_w(x) = T_f = T_\infty + bx$ where $T_\infty$ is the temperature of the ambient fluid, $T_f$ is the temperature of convective heating, $T_w$ is the wall temperature, and $b$ is a constant. Assisting flow exist when a heated surface $T_w(x) > T_\infty$ when $b > 0$. Conversely, the plate is cooled ($b < 0$) as $T_w(x) < T_\infty$ and thus opposing flow occurs.

Following these assumptions together with Rosseland and Boussinesq approximation, neglecting the viscous dissipation effect, the governing equations (Ali et al., 2021) are

$$\frac{\partial u}{\partial x} + \frac{\partial v}{\partial y} = 0\,, \tag{1}$$

$$u\frac{\partial u}{\partial x} + v\frac{\partial u}{\partial y} = -\frac{1}{\rho}\frac{dp}{dx} + \nu\frac{\partial^2 u}{\partial y^2} - \frac{\sigma_e \mu_e^2 H_0^2}{\rho}u + g\beta(T - T_\infty)\,, \tag{2}$$

$$u\frac{\partial T}{\partial x} + v\frac{\partial T}{\partial y} = \frac{k}{\rho c_p}\frac{\partial^2 T}{\partial y^2} - \frac{1}{\rho c_p}\frac{\partial q_r}{\partial y}\,. \tag{3}$$

These equations (1)-(3) are subjected to the boundary conditions:

$$\begin{aligned} &v = 0, \quad u = u_w(x) = cx, \ -k\frac{\partial T}{\partial y} = h_f\left(T_f - T\right) \ \text{ at } y = 0, \\ &u = u_e(x) = ax, \quad T = T_\infty \quad \text{as } y \to \infty, \end{aligned} \tag{4}$$

where $u$ and $v$ are the velocity components along the $x$ and $y$ axes, respectively. The fluid temperature is $T$, $g$ is the acceleration due to gravity, $p$ is the fluid pressure, $T_f$ is the temperature from convective heating, $h_f$ is convective heat transfer coefficient and $q_r, \mu_e, \sigma_e, \beta, \rho, \nu, c_p$ and $k$ are the Rosseland approximation for radiation, the magnetic permeability, the electrical conductivity, the thermal expansion coefficient, the fluid density, the kinematic viscosity, the specific heat of the fluid at a constant pressure, and the thermal conductivity, respectively.

Raptis et al. (2004) suggested to substitute $q_r = -\frac{4\sigma^*}{3k^*}\frac{\partial T^4}{\partial y}$ into Eq. (3), with $q_r$ is the radiative heat flux, $k^*$ is the mean absorption coefficient and $\sigma^*$ is the Stefan-Boltzmann constant. Since $T^4$ can be written as a linear function of temperature $T$ using a truncated Taylor series about the free stream temperature due to the assumption that the difference of the temperature within the flow is sufficiently small, thus $T^4 \approx 4T_\infty^3 T - 3T_\infty^4$. Therefore, Eq. (3) becomes

$$u\frac{\partial T}{\partial x} + v\frac{\partial T}{\partial y} = \alpha\frac{\partial^2 T}{\partial y^2} - \frac{16\sigma^* T_\infty^3}{3k^*\rho C_p}\frac{\partial^2 T}{\partial y^2}. \tag{5}$$

In this study, nonlinear partial differential Eqs. (1), (2) and (5) are reduced to nonlinear ordinary differential equations using the same similarity transformation in Ali et al. (2021) and Makinde and Aziz (2011):

$$\varphi = x\sqrt{a\nu}f(\eta), \qquad \eta = \sqrt{\frac{a}{\nu}}y, \qquad \theta(\eta) = \frac{T - T_\infty}{T_f - T_\infty}, \tag{6}$$

where φ is the stream function, $\eta$ is the similarity variable and $\theta$ is the non-dimensional temperature.

By applying Eq. (6), Eq. (1) is satisfied, while Eqs. (2) and (5) are reduced to the following ordinary differential equation (ODE):

$$f''' + ff'' - f'^2 + 1 + Ha^2(1 - f') + \lambda\theta = 0, \tag{7}$$

$$\frac{1}{Pr}\left(1 + \frac{4}{3}Rd\right)\theta'' + f\theta' - f'\theta = 0, \tag{8}$$

with the new boundary conditions

$$\begin{aligned} f(0) = 0, \ \ f'(0) = A, \ \ -\theta'(0) = Bi(1 - \theta(0)), \\ f'(\infty) \to 1, \ \theta(\infty) \to 0. \end{aligned} \tag{9}$$

From Eqs. (7) - (9),

$$Ha = \mu_e H_0\sqrt{\frac{\sigma_e}{\rho a}}, \ \lambda = \frac{Gr_x}{Re_x^2}, Pr = \frac{\mu c_p}{k}, \ Rd = \frac{4\sigma^* T_\infty^3}{kk^*}, \ A = \frac{c}{a}, \ Bi = \frac{h_f}{k}\sqrt{\frac{\nu}{a}} \tag{10}$$

are the Hartmann number, the mixed convection or buoyancy parameter, the Prandtl number, the radiation parameter, the wall ratio velocity parameter and the Biot number, respectively and $\mu$ is the dynamic viscosity (Ali et al., 2021; Makinde and Aziz, 2011).

The physical quantities of interest are the skin friction coefficient, $C_f$ and the local Nusselt number, $Nu_x$, which are defined as in Ali et al. (2021)

$$C_f = \frac{\tau_w}{\frac{1}{2}\rho u_e^2} \quad , \quad Nu_x = \frac{x q_w}{k(T_w - T_\infty)}, \tag{11}$$

with $\tau_w$ is the surface shear stress and $q_w$ is the surface heat flux. From Bakar et.al (2018), we define

$$\tau_w = \mu\left(\frac{\partial u}{\partial y}\right)_{y=0}, \; q_w = -\left(k + \frac{16\sigma^* T_\infty^3}{3k^*}\right)\left(\frac{\partial T}{\partial y}\right)_{y=0}, \tag{12}$$

and simplify the equations (12), we obtain

$$Re_x^{1/2} C_f = 2f''(0), \; Re_x^{-1/2} Nu_x = -\left(1 + \tfrac{4}{3}Rd\right)\theta'(0). \tag{13}$$

## RESULTS AND DISCUSSION

The set of the ordinary differential Eqs. (7) and (8) with the boundary conditions (9) have been solved numerically using bvp4c method in MATLAB software. A numerical comparison with the study done by Ali et al. (2014, 2021) for the case of assisting flow ($\lambda > 0$) and opposing flow ($\lambda < 0$) has been done. The values of the skin friction coefficient, $f''(0)$ and the local Nusselt number, $-\theta'(0)$ are obtained for the case of $A = 1$ when the Hartmann number and radiation parameter are absent. A large Biot number, $Bi$ is used to check the validity of the numerical results as suggested by Makinde and Aziz (2011). The stretching sheet at a constant temperature were recovered by using a large $Bi$ value which reduced the boundary condition, $\theta(0) = 1$ (isothermal condition). It is good to mentioned that Ali et al. (2014) used Keller box method, while Ali et al. (2021) used bvp4c method to solve their problems.

**Table 1:** The skin friction coefficient, $f''(0)$ and the local Nusselt number, $-\theta'(0)$ for different values of $Pr$ when $A = 1$, $Ha = 0$, $Rd = 0$, $Bi = 10000$ and $\lambda = 1$

| | Ali et al. (2014) | | Ali et al. (2021) | | Present | |
|---|---|---|---|---|---|---|
| $Pr$ | $f''(0)$ | $-\theta'(0)$ | $f''(0)$ | $-\theta'(0)$ | $f''(0)$ | $-\theta'(0)$ |
| 0.72 | 0.3645 | 1.0931 | 0.3645 | 1.0931 | 0.3645 | 1.0932 |
| 6.8 | 0.1804 | 3.2897 | 0.1804 | 3.2896 | 0.1805 | 3.2907 |
| 20 | 0.1175 | 5.6208 | 0.1175 | 5.6201 | 0.1178 | 5.6233 |
| 40 | 0.0873 | 7.9403 | 0.0873 | 7.9383 | 0.0873 | 7.9446 |
| 60 | 0.0729 | 9.7217 | 0.0728 | 9.7180 | 0.0729 | 9.7275 |
| 80 | 0.0640 | 11.2244 | 0.0639 | 11.2187 | 0.0640 | 11.2314 |
| 100 | 0.0578 | 12.5490 | 0.0577 | 12.5411 | 0.0578 | 12.5569 |

**Table 2:** The skin friction coefficient, $f''(0)$ and the local Nusselt number, $-\theta'(0)$ for different values of $Pr$ when $A = 1$, $Ha = 0$, $Rd = 0$, $Bi = 10000$ and $\lambda = -1$

| | Ali et al. (2014) | | Ali et al. (2021) | | Present | |
|---|---|---|---|---|---|---|
| $Pr$ | $f''(0)$ | $-\theta'(0)$ | $f''(0)$ | $-\theta'(0)$ | $f''(0)$ | $-\theta'(0)$ |
| 0.72 | -0.3852 | 1.0293 | -0.3852 | 1.0293 | -0.3852 | 1.0293 |
| 6.8 | -0.1832 | 3.2463 | -0.1832 | 3.2461 | -0.1832 | 3.2471 |
| 20 | -0.1183 | 5.5903 | -0.1183 | 5.5896 | -0.1183 | 5.5927 |

| | | | | | | |
|---|---|---|---|---|---|---|
| 40 | -0.0876 | 7.9169 | -0.0876 | 7.9145 | -0.0876 | 7.9211 |
| 60 | -0.0731 | 9.7018 | -0.0730 | 9.6982 | -0.0731 | 9.7075 |
| 80 | -0.0641 | 11.2068 | -0.0641 | 11.2012 | -0.0641 | 11.2137 |
| 100 | -0.0579 | 12.5329 | -0.0578 | 12.5252 | -0.0579 | 12.5408 |

Tables 1 and 2 show the published and present results for both skin friction coefficient and local Nusselt number, respectively. The comparison achieved an excellent agreement for both assisting and opposing flow cases. The results show good agreement for the skin friction coefficient, however good agreement for the local Nusselt number occur for small Prandtl number. It is observed that an increment of Prandtl number, $Pr$ will decrease the skin friction coefficient, $f''(0)$. The opposite phenomenon happens to the heat transfer rate at the surface, $-\theta'(0)$.

The ratio of the internal thermal resistance of a solid to the boundary layer thermal resistance is measured by the Biot number, $Bi$. The left side of the plate containing the hot fluid is completely insulated due to the non-existence of Biot number when $Bi = 0$. The plate's internal thermal resistance is very high, and no convective heat transfer to the cold fluid on the right side of the plate take place (Makinde and Aziz, 2010). Figure 2 shows the velocity profile with and without Biot number. It is noticeable that the profile shifts upward as $Bi$ increase, indicating an increment of the velocity gradients. A significant movement is shown as the Biot number increases to a certain value.

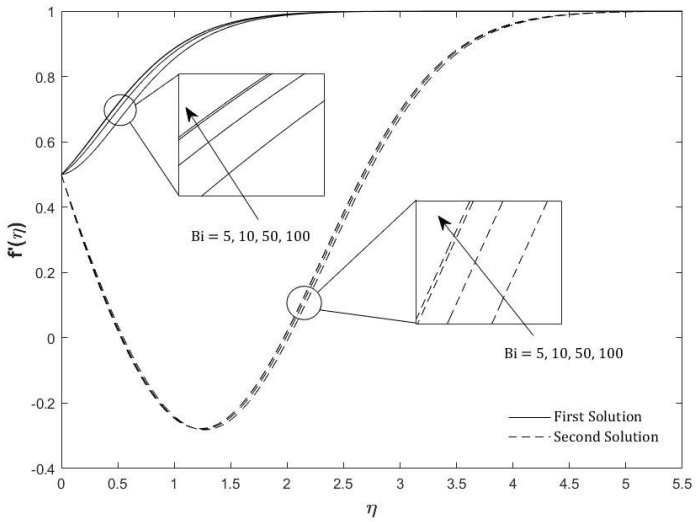


**Figure 2:** Velocity profile for various $Bi$ when $A$ = 0.5, $Pr$ = 6.8, $Ha$ = 1, $Rd$ = 0.6 and $\lambda = -2$.

In this study, the results for velocity profiles, temperature profiles, skin friction coefficient and Nusselt number are mostly only considered when $A < 1$ due to similar results obtained for $A > 1$. It is good to mention that higher $Bi$ implies a stronger convective heat transfer, which enhances the momentum transfer within the fluid, leading to a higher velocity near the boundary. Therefore, Figures 2 and 3 illustrate the effect of large Biot number on the velocity profiles and temperature profiles when the wall ratio velocity parameter, $A < 1$. Both profiles satisfy the boundary condition (9). The effect of $Bi$ on the velocity and temperature profiles produce dual branches (first and second solutions). The velocity profiles (in Figure 2) for the first solution are discovered to

increase as $Bi$ increases, which is found to be the same for the second solution. The dual profiles also produced when the flow is opposing. While from Figure 3, increasing $Bi$ value suggest that the temperature profile decreases significantly. When the Biot number is too large, the temperature profile (for the first solution) shifted and getting closer to the boundary.

Figures 4 and 5 display the skin friction coefficient and the local Nusselt number for various values of $Bi$ and $\lambda$, respectively. Dual solutions exist for opposing flow only. For upper solution, the skin friction coefficient exhibits a changing behaviour for increasing $Bi$. For assisting flow, Biot number reduces the skin friction coefficient while the skin friction coefficient increases with Biot number for opposing flow. However, the local Nusselt number is observed to reduce with $Bi$ for both flows.

The second solutions exist in the opposing flow regime for both skin friction coefficient and local Nusselt number until certain critical values denoted as $\lambda_{c_i}$ for $i = 1, 2, 3, 4$. Second solutions show increasing behaviour for the skin friction coefficient, until a certain opposing flow range. A transition effect is then observed where the second solutions decrease with large $Bi$ values. This transition effect also has been depicted for the second solutions of the local Nusselt number, which increases along high Biot number. Increasing values in Biot number have expanding the range of solutions. It is observed that the skin friction coefficient and the local Nusselt number have no solution when $\lambda < |\lambda_c|$, where $\lambda_c$ is the critical value. It can be observed from Figures 4 and 5 that $\lambda_c = -6.333246, -7.30659, -8.12610, -8.23$ for $Bi = 5, 10, 50, 100$, respectively. Thus, the boundary layer separation occurs beyond these critical values. This indicates that Biot number delays the boundary layer separation. By delaying the boundary layer separation, drag will be reduced, hence this can improve the aerodynamic performance of any object moving through fluids, such as aircraft wings.

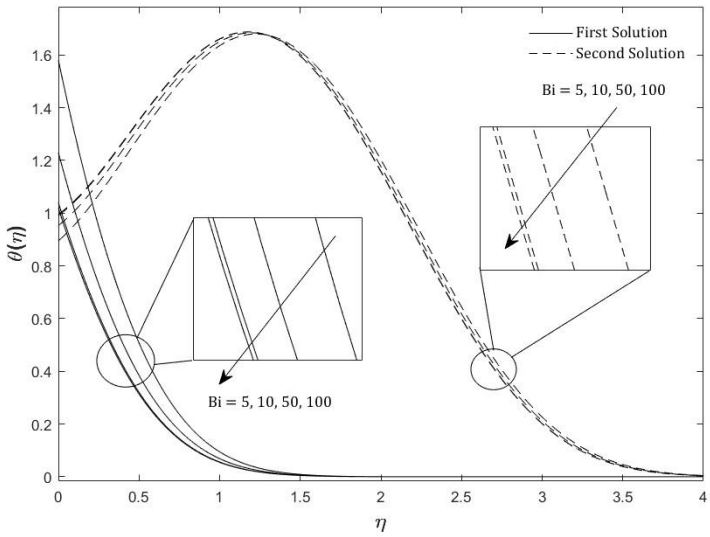


**Figure 3:** Temperature profile for various $Bi$ when $A = 0.5$, $Pr = 6.8$, $Ha = 1$, $Rd = 0.6$ and $\lambda = -2$

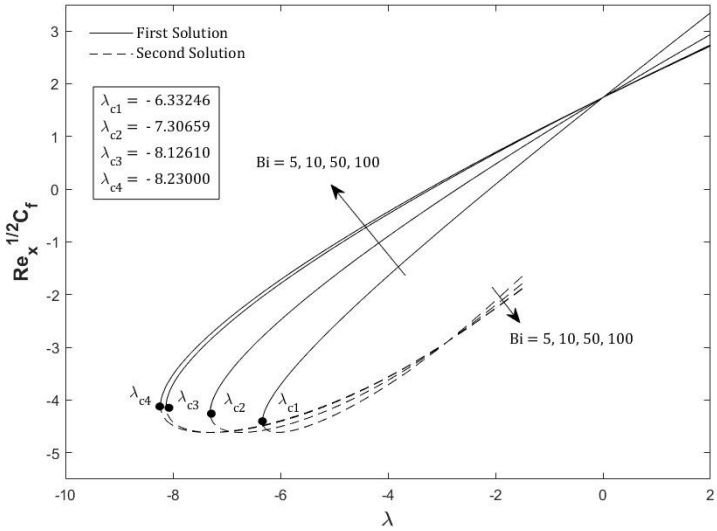


**Figure 4:** Skin friction coefficient for various $Bi$ when $A = 0.5$, $Pr = 6.8$, $Ha = 1$, and $Rd = 0.6$

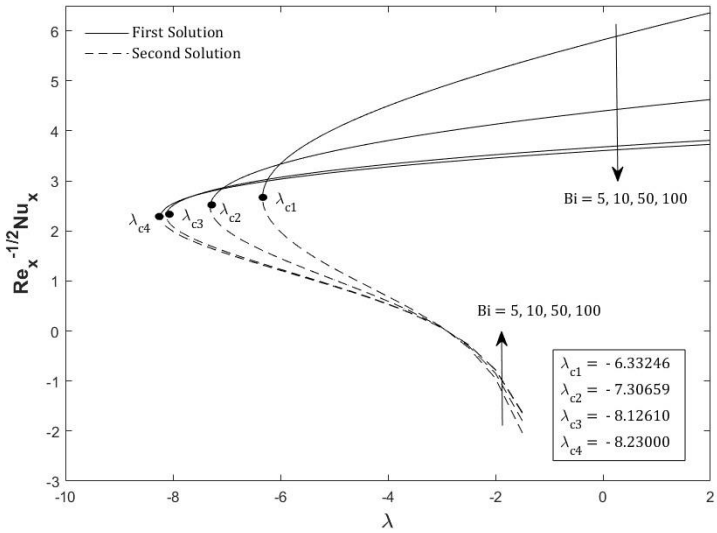


**Figure 5:** Local Nusselt number for various $Bi$ when $A = 0.5$, $Pr = 6.8$, $Ha = 1$, and $Rd = 0.6$

Figure 6 illustrates the temperature profiles for different values of radiation parameter, $Rd$ which shows dual temperature profiles exist when $\lambda = -3$. Thus, dual solutions exist for the case of opposing flow. The temperature profile increases with $Rd$ for both first and second solutions.

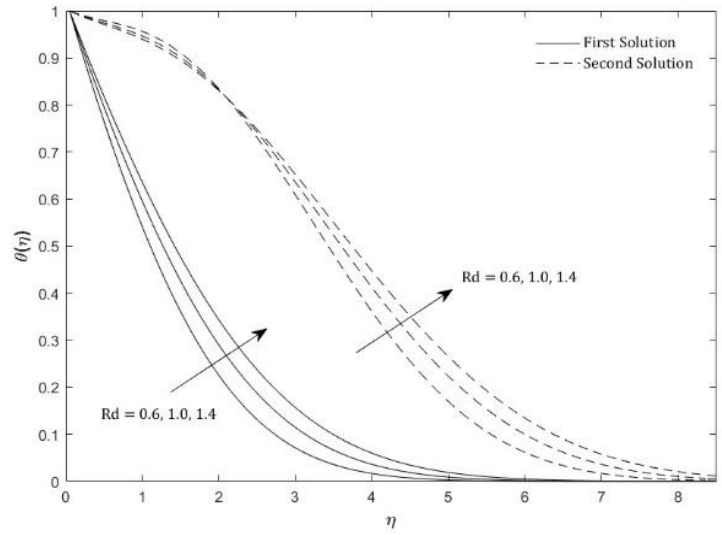


**Figure 6:** Temperature profile for various *Rd* when $A = 0.5$, $Pr = 0.72$, $Ha = 1$, $Bi = 20$ and $\lambda = -3$

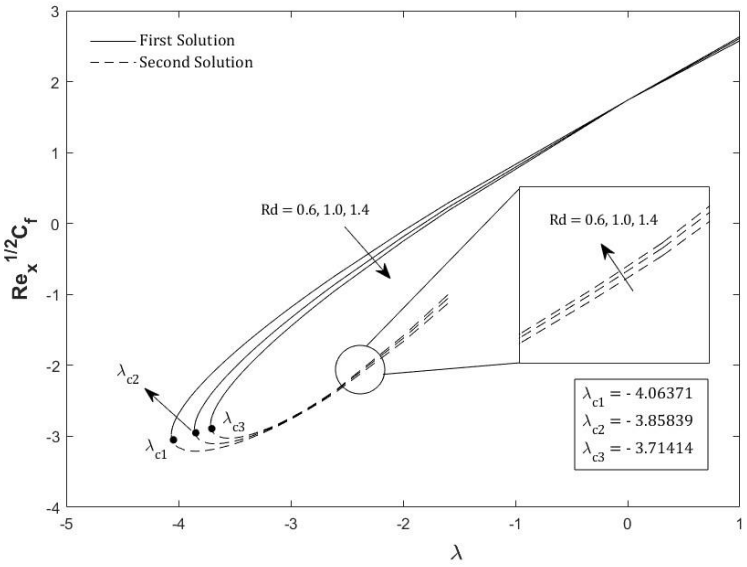


**Figure 7:** Skin friction coefficient as a function of $\lambda$ for various $Rd$ when $A = 0.5$, $Pr = 0.72$, $Ha = 1$ and $Bi = 20$

Plotted skin friction coefficient and local Nusselt number for different radiation parameter *Rd* are shown in Figures 7 and 8, respectively. The smooth upper branch in both Figures 7 and 8 are the first solution while the lower branch is the second solution. Adding values of *Rd* shows an increase skin friction coefficient for the second solutions, which totally in contrast with the first solutions. The local Nusselt number also achieves contrast behaviour for the first and second solutions with certain values of $\lambda$. Growing value in *Rd* has shorten the range of $\lambda$ which is believed to be no solution beyond the critical values for the skin friction coefficient and the local Nusselt number, respectively. Thus, larger values of radiation parameter will enhance the boundary layer separation to occur.

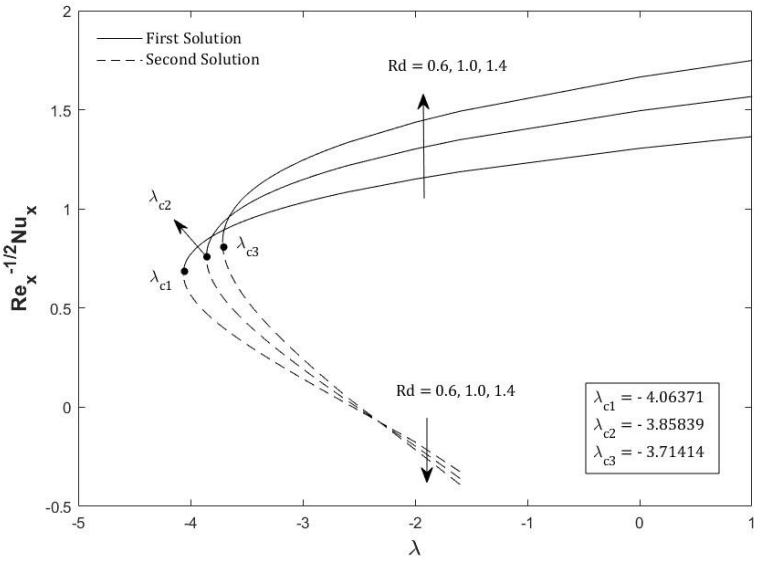


**Figure 8:** Local Nusselt number as a function of $\lambda$ for various $Rd$ when $A = 0.5$, $Pr = 0.72$, $Ha = 1$ and $Bi = 20$

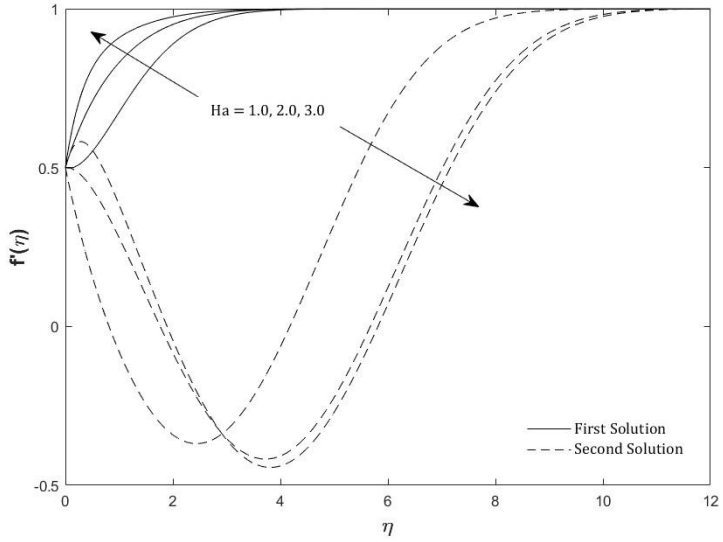


**Figure 9:** Velocity profile for various $Ha$ when $A = 0.5$, $Pr = 0.72$, $Rd = 0.6$, $Bi = 20$ and $\lambda = -2$

The effect of Hartmann number on the velocity and temperature profiles can be found in Figures 9 and 10. Dual solutions exist for opposing flows. As the Hartmann number increases, the velocity profile increases for the first solutions and decreases for the second solutions. The temperature profile exhibits different results. Increasing Hartmann number lower the temperature profile for the first solution as depicted in the magnify picture in Figure 10. The second solutions are observed to increase along with the Hartmann number.

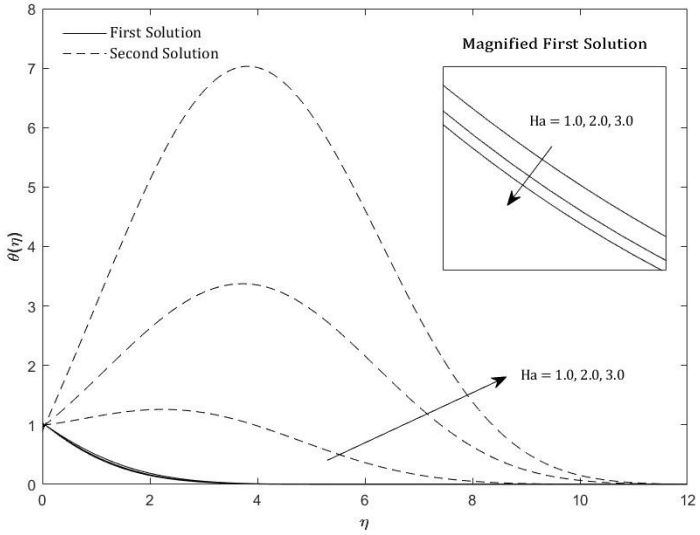


**Figure 10:** Temperature profile for various *Ha* when $A = 0.5$, $Pr = 0.72$, $Rd = 0.6$, $Bi = 20$ and $\lambda = -2$

Increment in Hartmann number has significant effect to the skin friction coefficient and the local Nusselt number. Figure 11 displays the skin friction coefficient, $\mathrm{Re_x}^{1/2}\mathrm{C_f}$ as a function of $\lambda$ for different values of the Hartmann number, namely $Ha = 1.0, 2.0, 3.0$. The solid line indicates the first solution, while the dashed line indicates the second solution. It is observed that the first solution exists only for $\lambda > 0$ until certain range of $\lambda < 0$. The critical points denoted as $\lambda_{c1}$, $\lambda_{c2}$, $\lambda_{c3}$ marked where the curves exhibit changes which correspond to the onset of multiple solutions. As *Ha* increases, the curves shift upward, indicating a higher skin friction coefficient for the same $\lambda$. Higher values of *Ha* produce wider range of solutions compared to lower *Ha*. Physically, this suggests that a stronger magnetic field stabilizes the flow and increases surface drag.

The graph in Figure 12 shows the local Nusselt number, $Re_x{}^{-1/2}Nu_x$ as a function of $\lambda$ for various values of the Hartmann number, *Ha*. Dual solutions are obtained with the first solution as the upper branch and the second solution is the lower branch. A smooth increase in the Nusselt number with decreasing $\lambda$ was illustrated for the first solution. The heat transfer increases significantly as $\lambda$ becomes larger. The second solution exhibits a more complex behaviour, with the Nusselt number decreasing sharply for smaller values of $\lambda$. This suggests that the second solution becomes unstable or physically unrealistic in certain regions. The critical points are identified where the behaviour of the solution changes. An upward movement of the curves are observed as *Ha* increases. This demonstrates that higher *Ha* increases the heat transfer at the surface. Increasing the Hartmann number, *Ha* stabilizes the flow and enhances heat transfer, as indicated by the rise in the local Nusselt number. The Hartmann number are known related to the Lorentz force, whereby, when *Ha* increases, the Lorentz force also increases (Ali et al., 2021). This suggest that the momentum of the fluid flow will slow down, and hence, increase the drag at the surface. Therefore, the skin friction coefficient and the local Nusselt number increases. The Hartmann number found to delay the boundary layer separation and broaden the range of $\lambda$. Dual solutions found for opposing flow, whereas, for assisting flow, only unique solution observed.

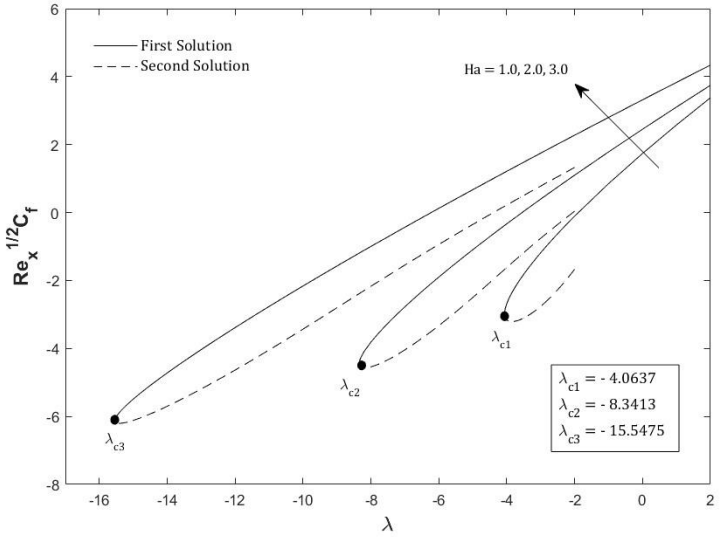


**Figure 11:** Skin friction coefficient for various $Ha$ when $A = 0.5$, $Pr = 0.72$, $Rd = 0.6$ and $Bi = 20$

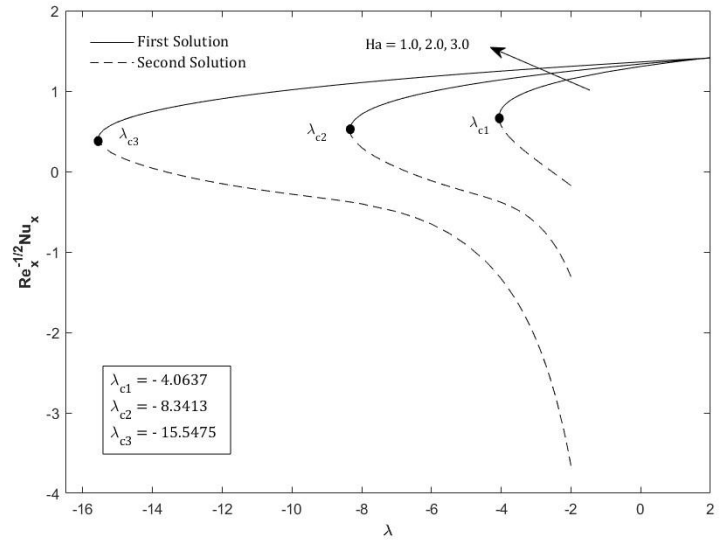


**Figure 12:** Local Nusselt number for various $Ha$ when $A = 0.5$, $Pr = 0.72$, $Rd = 0.6$ and $Bi = 20$

In the study of mixed convection flows, the relationship between the directions of the natural convection and forced convection are the main concern. These interactions significantly influence the flow dynamics and heat transfer characteristics. Assisting and opposing flows, when $A < 1$ is displayed in Figure 13 for different values of Prandtl number, $Pr$. Increasing $Pr$ values show that the thermal boundary layer thickness for opposing flow is larger compared to assisting flow.

Figure 14 displays the distinct effect of $A$ on velocity profiles for both assisting and opposing flows. The flow shows a boundary layer structure in the case of $A < 1$. On the other way, an inverted boundary layer structure is seen because of the stretching velocity of the surface exceeds the velocity of the free stream. As $A$ increases, it is also seen that the boundary layer thickness decreases. A significant effect for different buoyancy or mixed convection parameter, $\lambda$ is shown in Figure 15. Two types of lines, solid and dash line, indicate the first and second branch solutions for the velocity profile. Different colours are used to distinguish assisting flow (black) and

opposing flow (blue) cases. Unique solutions are obtained for the case of $\lambda = 0$, 1, 2 and 3, while dual solutions exist for $\lambda < 0$. Larger values of $\lambda$ will produce larger buoyancy force, which produce larger kinetic energy, which helps to reduce resistant of the fluid flow (Ali et al., 2014).

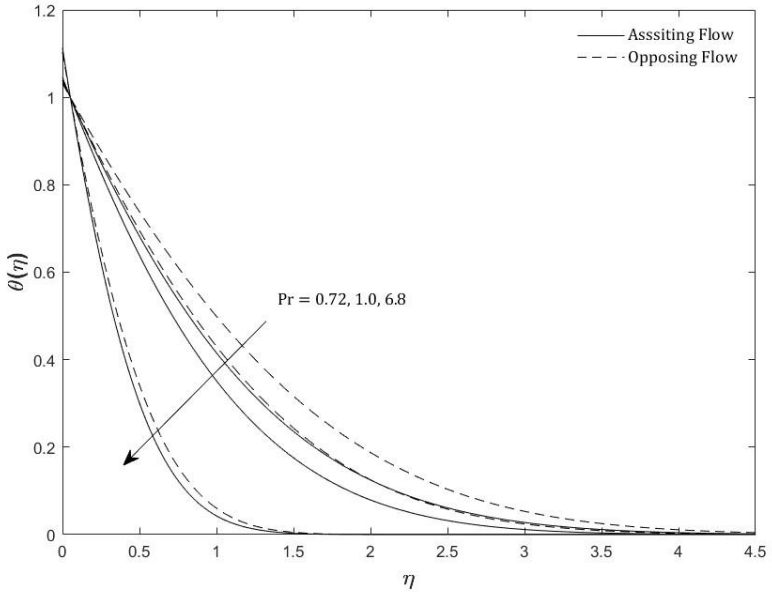


**Figure 13:** Temperature profile for various *Pr* when $A = 0.5$, $Ha = 1$, $Rd = 0.6$, $Bi = 20$ for assisting flow and opposing flow

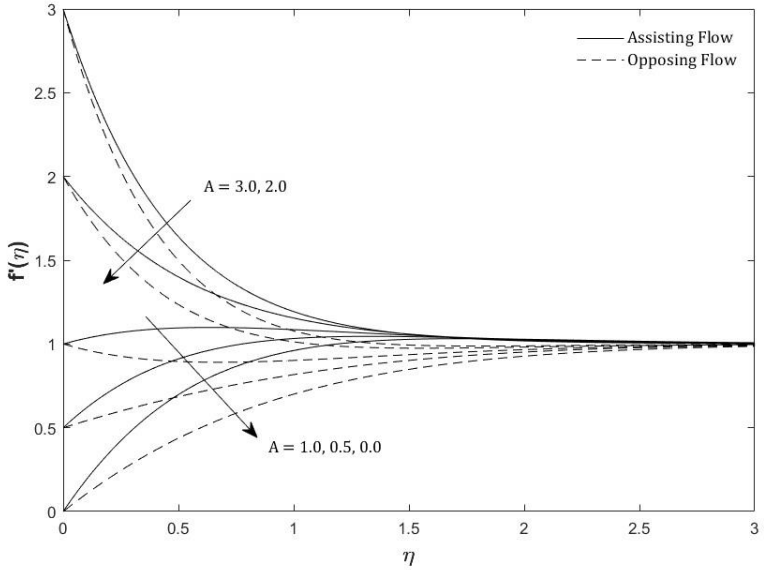


**Figure 14:** Velocity profile for various $A$ when $Pr = 0.72$, $Ha = 1$, $Rd = 0.6$ and $Bi = 20$ for $\lambda = 1$ (assisting flow) and $\lambda = -1$ (opposing flow)

Figure 16 describes the velocity profiles when $A < 1$ and $A > 1$ for different cases of $\lambda$. The solid lines represent $A = 2.0$, while the dashed lines indicate $A = 0.5$, holding other parameters with fixed values. Black lines represent assisting flow, while blue lines are opposing flows. A significant difference can be observed for the velocity profile. Reversed phenomenon occurs for the mixed convection parameter. The profile increases for assisting flows despite the changes in $A$. However, opposite trend is found in the opposing flow. Boundary layer structure and inverted

boundary layer structure can be seen where the boundary layer thickness is larger for $A < 1$, compared to the thickness when $A > 1$, and also larger for the opposing flow.

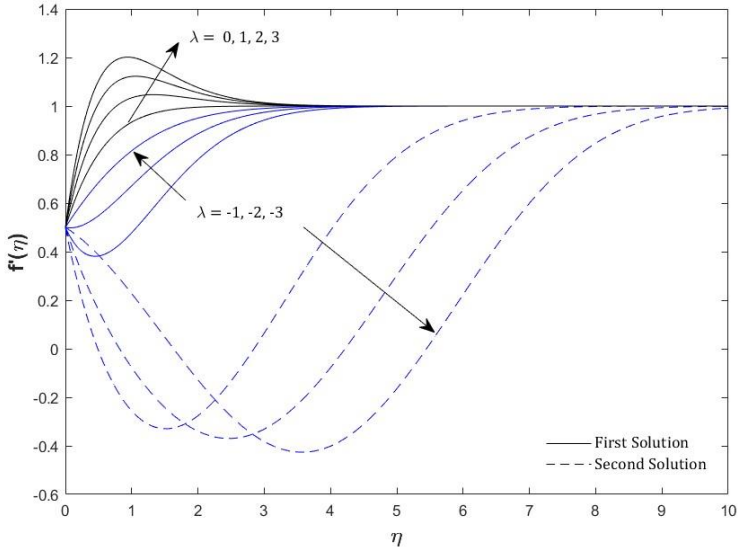


**Figure 15:** Velocity profile for various $\lambda$ when $A = 0.5$, $Pr = 0.72$, $Ha = 1$, $Rd = 0.6$ and $Bi = 20$

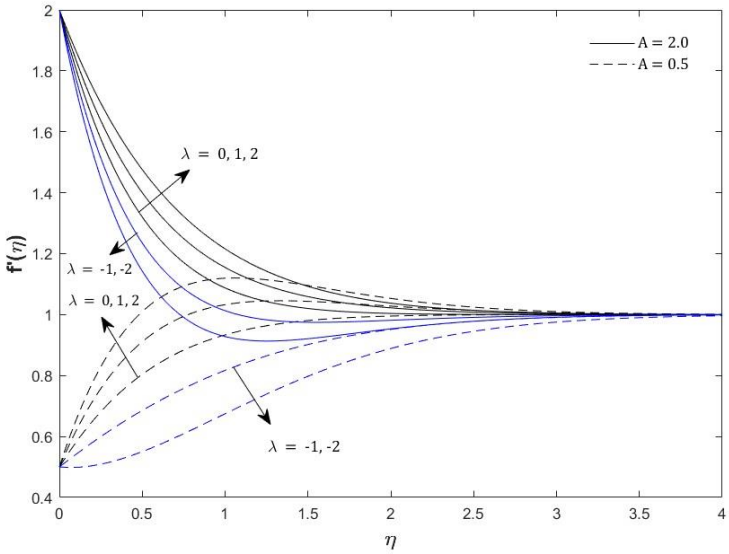


**Figure 16:** Velocity profile for various $\lambda$ when $Pr = 0.72$, $Ha = 1$, $Rd = 0.6$ and $Bi = 20$ for both $A = 0.5$ and $A = 2.0$

## CONCLUSION

A numerical study on the mixed convection stagnation-point flow of an incompressible viscous fluid over a stretching sheet in the presence of an externally magnetic field with consideration towards convective boundary condition and radiation effect is performed. The conclusions for the present study are as follows:

- The wall ratio velocity parameter reduces the velocity profile when its value become smaller.
- Dual solutions are found to exist for opposing flow and unique solution exist for assisting flow.
- Biot number shows a significant impact on the velocity profile and temperature profile as the values increase.
- Too large Biot number only shows the profile getting closer to the boundary.
- The skin friction coefficient and local Nusselt number with higher Biot number and Hartmann number produce wider range of solutions. Thus, the Biot number and Hartmann number delay the boundary layer separation. The delay can be applied in engineering as a tool in thermal management and energy-related technologies.
- However, the radiation parameter enhances the boundary layer separation.

## REFERENCES

Akbar, N. S., Nadeem, S., Haq, R. U. and Khan, Z. (2013), Radiation effects on MHD stagnation point flow of nano fluid towards a stretching surface with convective boundary condition. *Chinese Journal of Aeronautics*, **26(6)**: 1389–1397.

Ali, F. M., Khamat, A. N. A. and Junoh, M. M. (2021), Dual solutions in mixed convection stagnation-point flow over a vertical stretching sheet with external magnetic field and radiation effect. *Journal of Advanced Research in Fluid Mechanics and Thermal Sciences*, **80(2)**: 22–32.

Ali, F. M., Nazar, R., Arifin, N. M. and Pop, I. (2011), MHD boundary layer flow and heat transfer over a stretching sheet with induced magnetic field. *Heat and Mass Transfer*, **47**:155–162.

Ali, F. M., Nazar, R., Arifin, N. M. and Pop, I. (2014), Mixed convection stagnation point flow on vertical stretching sheet with external magnetic field. *Applied Mathematics and Mechanics*, **35(2)**: 155–166.

Arulmozhi, S., Sukkiramathi, K., Santra, S. S., Edwan, R., Fernandez-Gamiz, U. and Noeiaghdam, S. (2022), Heat and mass transfer analysis of radiative and chemical reactive effects on MHD nanofluid over an infinite moving vertical plate. *Results in Engineering*, **14**: 100394.

Aziz, A. (2009), A similarity solution for laminar thermal boundary layer over a flat plate with a convective surface boundary condition. *Communications in Nonlinear Science and Numerical Simulation*, **14(4)**: 1064–1068.

Bakar, S. A., Arifin, N. M., Nazar, R., Ali, F. M., Bachok, N. and Pop, I. (2018), The effects of suction on forced convection boundary layer stagnation point slip flow in a Darcy porous

medium towards a shrinking sheet with presence of thermal radiation: A stability analysis. *Journal of Porous Media*, **21(7)**: 623–636.

Das, K. (2014), Radiation and melting effects on MHD boundary layer flow over a moving surface. *Ain Shams Engineering Journal*, **5(4)**: 1207–1214.

Ferdows, M., Shamshuddin, M., Salawu, S. and Reza, M. (2022), Computation of heat transfer in magnetised Blasius flow of nano-fluids with suspended carbon nanotubes through a moving flat plate. *International Journal of Ambient Energy*, **43(1)**: 7657–7665.

Hayat, T., Qayyum, S., Alsaedi, A. and Asghar, S. (2017), Radiation effects on the mixed convection flow induced by an inclined stretching cylinder with non-uniform heat source/sink. *PLoS One*, **12(4)**: e0175584.

Ishak, A. (2011), MHD boundary layer flow due to an exponentially stretching sheet with radiation effect. *Sains Malaysiana*, **40(4)**: 391–395.

Makinde, O. D. and Aziz, A. (2010), MHD mixed convection from a vertical plate embedded in a porous medium with a convective boundary condition. *International Journal of Thermal Sciences*, **49(9)**: 1813–1820.

Makinde, O. D. and Aziz, A. (2011), Boundary layer flow of a nanofluid past a stretching sheet with a convective boundary condition. *International Journal of Thermal Sciences*, **50(7)**: 1326–1332.

Motozawa, M., Chang, J., Sawada, T. and Kawaguchi, Y. (2010), Effect of magnetic field on heat transfer in rectangular duct flow of a magnetic fluid. *Physics Procedia*, **9**: 190–193.

Raptis, A., Perdikis, C. and Takhar, H. S. (2004), Effect of thermal radiation on MHD flow. *Applied Mathematics and Computation*, **153(3)**: 645–649.

Reddy, P. S., Sreedevi, P. and Chamkha, A. J. (2018), Magnetohydrodynamic (MHD) boundary layer heat and mass transfer characteristics of nanofluid over a vertical cone under convective boundary condition. *Propulsion and Power Research*, **7(4)**: 308–319.

Seddeek, M. (2002), Effects of radiation and variable viscosity on a MHD free convection flow past a semi-infinite flat plate with an aligned magnetic field in the case of unsteady flow. *International Journal of Heat and Mass Transfer*, **45(4)**: 931–935.

Yahaya, R. I., Mustafa, M. S., Arifin, N. M., Pop, I., Wahid, N. S., Ali, F. M. and Mohamed Isa, S. S. P. (2024), Mixed convection hybrid nanofluid flow over a stationary permeable vertical cone with thermal radiation and convective boundary condition. *ZAMM-Journal of Applied Mathematics and Mechanics*, **104(4)**: page e202300428.